

# Stochastic IMT (insulator-metal-transition) neurons: An interplay of thermal and threshold noise at bifurcation

Abhinav Parihar,<sup>1</sup> Matthew Jerry,<sup>2</sup> Suman Datta,<sup>2</sup> and Arijit Raychowdhury<sup>1</sup>

<sup>1</sup>Georgia Institute of Technology, Atlanta, GA

<sup>2</sup>University of Notre Dame, Notre Dame, IN

A stochastic neuron, a key hardware kernel for implementing stochastic neural networks, is constructed using an insulator-metal-transition (IMT) device based on electrically induced phase-transition in series with a tunable resistance. We show that such an IMT neuron has dynamics similar to a piecewise linear FitzHugh-Nagumo (FHN) neuron. Spiking statistics of such neurons are demonstrated experimentally using Vanadium Dioxide (VO<sub>2</sub>) based IMT neurons, and modeled as an Ornstein-Uhlenbeck (OU) process with a fluctuating boundary. The stochastic spiking is explained by thermal noise and threshold fluctuations acting as precursors of bifurcation which result in a sigmoid-like transfer function. Moments of interspike intervals are calculated analytically by extending the first-passage-time (FPT) models for Ornstein-Uhlenbeck (OU) process to include a fluctuating boundary. We find that the coefficient of variation of interspike intervals depend on the relative proportion of thermal and threshold noise. In the current experimental demonstrations where both kinds of noise are present, the coefficient of variation is about an order of magnitude higher compared to the case where only thermal noise were present.

A growing need for efficient machine-learning in autonomous systems coupled with an interest in solving computationally hard optimization problems has led to active research in stochastic models of computing. Optimization techniques [1] including Stochastic Sampling Machines (SSM), Simulated Annealing, Stochastic Gradients etc. are examples of such models. All these algorithms are currently implemented using digital hardware which first creates a mathematically accurate platform for computing, and later adds digital noise at the algorithm level. Hence, it is enticing to construct hardware primitives that can harness the already existing physical sources of noise to create a stochastic computing platform. The principal challenge with such efforts is the lack of stable or reproducible distributions, or functions of distributions, of physical noise. One basic stochastic unit which enables a systematic construction of stochastic hardware has long been known - the stochastic neuron [2] - which is also believed to be the unit of computation in the human brain. Moreover, recent studies [3] have demonstrated practical applications like sampling using networks of such stochastic spiking neurons. Here, we demonstrate and analytically study a stochastic neuron [4] which is fabricated using oscillators [5–7] based on insulator-to-metal transition (IMT) materials, e.g. Vanadium Dioxide (VO<sub>2</sub>), wherein the inherent physical noise in the dynamics is used to implement stochasticity. We show that such an IMT neuron has similar dynamics as a piecewise linear FitzHugh-Nagumo (FHN) neuron with thermal noise along with threshold fluctuations as precursors of bifurcation resulting in a sigmoid-like transfer function for the neural firing rates. By analyzing the variance of interspike interval, we determine that for the range of thermal noise present in our experimental demonstrations, threshold fluctuations are responsible for most of the stochasticity compared to thermal noise.

A stochastic IMT neuron is fabricated using relaxation oscillators [5, 7] composed of an IMT device, e.g. Vanadium Dioxide (VO<sub>2</sub>), in series with a tunable resistance, e.g. transistor [6] (Figure 1a). An IMT device is a two terminal device

with two resistive states - insulating (I) and metallic (M), and the device transitions between the two states based on the applied electric field (which in turn changes the current through the device and the corresponding temperature) across it. The phase transitions are hysteretic in nature, which means that the IMT (insulator-to-metal) transition does not occur at the same voltage as the MIT (metal-to-insulator) transition. For a range of values of the series resistance, the resultant circuit shows spontaneous oscillations due to hysteresis and a lack of stable point [7]. Overall, the series resistance acts as a parameter for bifurcation between a spiking (or oscillating) state and a resting state of an IMT neuron.

The equivalent circuit model for an IMT oscillator is shown in Figure 1b with the hysteretic switching conductance  $g_{v(m/i)}$  ( $g_{vm}$  in metallic and  $g_{vi}$  in insulating state), a series inductance  $L$ , and a parallel internal capacitance  $C$ . Let the IMT and MIT thresholds of the device be denoted by  $v_h$  and  $v_l$  respectively, with  $v_h > v_l$ , and the current-voltage relationship of the hysteretic conductance be

$$v_i = h(i_i, s)$$

where  $h$  is a linear function and  $s$  is the state - metallic (M) or insulating (I).

The system dynamics is then given by:

$$\begin{aligned} L \frac{di_i}{dt} &= (v_{dd} - h(i_i, s)) - v_o \\ C \frac{dv_o}{dt} &= i_i - g_s v_o \end{aligned} \quad (1)$$

with  $i_i$  and  $v_o$  as shown in figure 1b.

In VO<sub>2</sub>, IMT and MIT transitions are orders of magnitude faster than RC time constants for oscillations based on frequency [8] and time-domain measurements for voltage driven [9] and photoinduced transitions [10]. As such, the change in resistance of the IMT device is assumed to be instantaneous. Figure 2a shows the phase space  $i_o \times v_i$ . This phase space is a projection of  $i_o \times v_i \times s$ , which in turn is a scaled  $v_o \times i_i \times s$

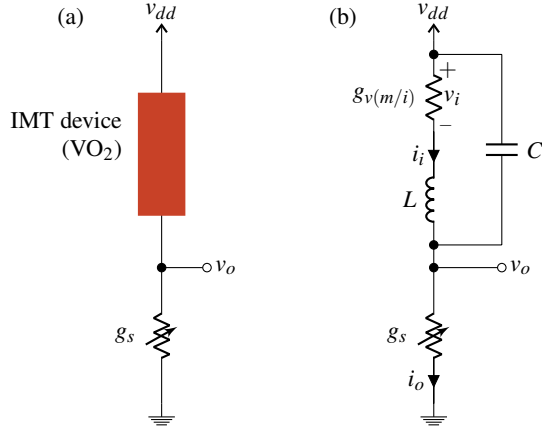


Figure 1. (a) VO<sub>2</sub> based IMT spiking neuron circuit consisting of a VO<sub>2</sub> device in series with a tunable resistance. (b) Equivalent circuit of IMT neuron using a series inductance  $L$  and a parallel capacitance  $C$

space as  $i_i = g_{v(m/i)}v_i$  and  $v_o = i_o/g_s$ . In steady state there is no current through the capacitor and no voltage drop across the inductor, and hence  $v_i = v_{dd} - v_o$  and  $i_i = i_o$ . V-I curves for IMT device in the two states metallic (M) and insulating (I) and the load line for series conductance  $v_i = v_{dd} - i_o/g_s$  are shown along with the fixed points of the system  $S_1$  and  $S_2$  in insulating and metallic states respectively. The load line and V-I curves are essentially the nullclines of  $v_o$  and  $i_i$  respectively. The capacitance-inductance pair delays the transitions and slowly pulls the system towards the fixed points  $S_1$  and  $S_2$  even when the IMT device transitions instantaneously. For large  $L/C$  ratio, the eigenvector with large negative eigenvalue becomes parallel to the  $x$ -axis, whereas the other eigenvector becomes parallel to  $AB'$  or  $BA'$  depending on the state (M or I). When the system is at A (or B) and IMT device is insulating (or metallic) with fixed point  $S_1$  (or  $S_2$ ), the IMT device transitions into metallic (or insulating) state changing the fixed point to  $S_2$  (or  $S_1$ ). Two trajectories are shown starting from points A and B each for the system (1) - one for large  $L/C$  value (solid) and the other for small  $L/C$  value (dashed). After a transition, the system moves parallel to  $x$ -axis almost instantaneously and spends most of the time following the V-I curve towards the fixed point. Before the fixed point is reached the MIT (or IMT) transition threshold is encountered which switches the fixed point, and the cycle continues resulting in sustained oscillations or spike generation.

For large  $L/C$ , an approximation can be made for the oscillating system without any hysteresis. The metallic and insulating states can be considered on either sides of the line  $AB$  (Figure 2a) because for large  $L/C$  the system always stays close to  $AB'$  or  $BA'$  whenever  $s$  transitions. As such, the function  $h$  can be written as a function of only  $v_o$  and  $i_i$  (or  $v_i$  and  $i_o$ ) without an explicit dependence on  $s$ . Furthermore, a coordinate transformation can be applied where  $y$ -axis is the same ( $v_i$ ), but  $x$ -axis is a linear function  $q(i_o, v_i)$  such that the boundary of metallic and insulating states ( $AB$ ) is parallel to  $y$ -axis

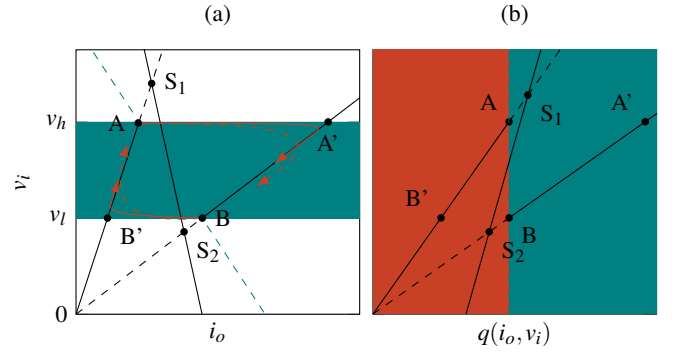


Figure 2. (a) Trajectories (red) of system (1) in the phase space  $i_o \times v_i$  for a large  $L/C$  value (solid) and a smaller  $L/C$  value (dashed). The  $i_i$ -nullclines of system (1) are shown as solid black lines in the metallic ( $AB'$ ) and insulating ( $BA'$ ) states of the IMT device, and  $S_1S_2$  is the  $v_o$ -nullcline. In the region where  $i_o(A) < i_o < i_o(B)$  the  $i_i$ -nullclines are dependent on  $s$  (b) IMT neuron system (1) in the transformed phase space  $q \times v_i$  have nullclines with similar characteristics as the McKean's caricature of FHN neuron model for large  $L/C$

(Figure 2b). This transforms equation (1) to the following form:

$$\begin{aligned} L_1 \frac{dq}{dt} &= (v_{dd} - h_1(q)) - kv_o \\ C \frac{dv_o}{dt} &= i_i - g_s v_o \end{aligned} \quad (2)$$

The model of (2) is very similar to a piecewise linear caricature of FitzHugh-Nagumo (FHN) neuron model [2], also called the McKean's caricature [11, 12]. Mathematically, the FHN model is given by:

$$\begin{aligned} \frac{du}{dt} &= f(u) - w + I_{ext} \\ \tau \frac{dw}{dt} &= u - bw + a \end{aligned} \quad (3)$$

where  $f(u)$  is a polynomial of third degree, e.g.  $f(u) = u - u^3/3$ , and  $I_{ext}$  is the parameter for bifurcation, as opposed to  $g_s$  in (2). In the FHN model, one variable ( $u$ ), possessing cubic nonlinearity, allows regenerative self-excitation via a positive feedback, and the second, a recovery variable ( $w$ ), possessing linear dynamics, provides a slower negative feedback. It was reasoned in Ref. 12 that the essential features of FHN model are retained in a "caricature" where the cubic non-linearity is replaced by a piecewise linear function which makes the  $u$ -nullcline in (3) similar to the  $q$ -nullcline in (2), which is the curve  $B'ABA'$  in figure 2b.

Bifurcation in VO<sub>2</sub> neuron is achieved by tuning the load line using a tunable resistance ( $g_s$ ), or a series transistor (figure 3a). Figure 3b shows two load line curves corresponding to different gate voltages ( $v_{gs}$ ), where one gives rise to spikes while the other results in a resting state. In the non-hysteretic approximation (system (2)), this bifurcation is a type of discontinuity induced bifurcation (DIB) involving piecewise smooth flows [13].

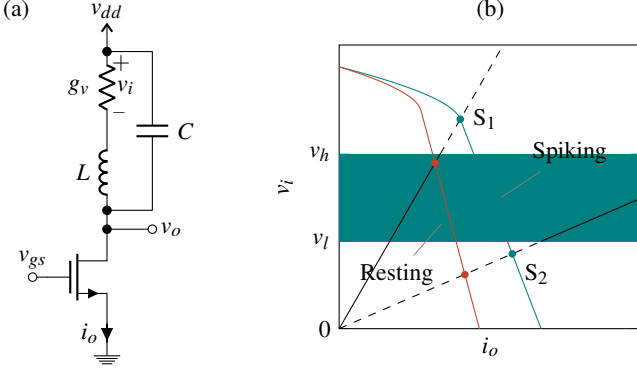


Figure 3. (a) IMT neuron with series transistor used to achieve bifurcation between a spiking and a resting state. (b) Nullclines of the system with series transistor in the phase space  $i_o \times v_i$  for two different  $v_{gs}$  values for spiking and resting states. Bifurcation occurs when a stable points crosses the boundary of region  $v_i \in [v_l, v_h]$ .

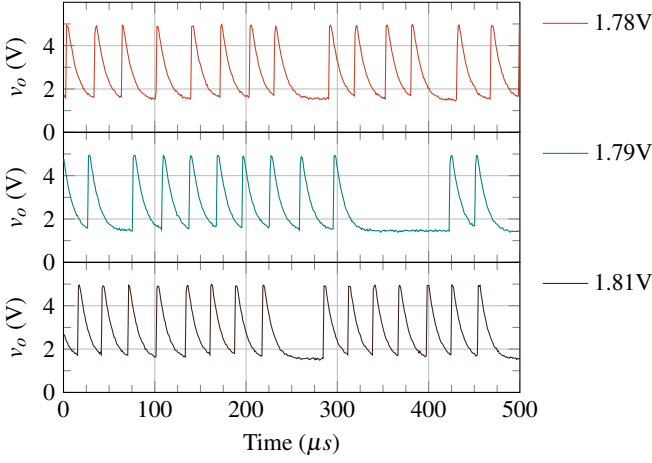


Figure 4. Experimental waveforms of VO<sub>2</sub> based spiking neuron for various  $v_{gs}$  values (1.78V, 1.79V and 1.81V). A VO<sub>2</sub> neuron shows almost instantaneous charging (spike) in metallic state.

Moreover, a single dimensional piecewise approximation of the system can be performed using a dimensionality reduction by replacing the movement along the eigenvector parallel to the x-axis with an instantaneous transition from A to A', or B to B'. This leaves a 1-dimensional subsystem in M and I each along the V-I curves AB' and BA'. Experiments using VO<sub>2</sub> show that the metallic state conductance  $g_{vm}$  is very high which causes the charging cycle of  $v_o$  to be almost instantaneous (figure 4) and resembles a spike of a biological neuron. As such, the spiking statistics can be studied by modeling just the discharge cycle of  $v_o$ . Also, in the insulating state, the current  $i_i$  does not vary due to low  $g_{vi}$ , and hence the inductance can be effectively removed and only the capacitance is needed for modeling the 1D subsystem of insulating state (figure 5a).

The two important noise sources which induce stochasticity in an IMT neuron are (a)  $V_{IMT}$  ( $v_h$ ) fluctuations [14, 15], and (b) thermal noise. Thermal noise  $\eta(t)$  is modeled in the cir-

cuit (figure 5a) as a white noise voltage  $\eta(t)dt = \sigma_t dw_t$  where  $w_t$  is the standard weiner process and  $\sigma_t^2$  is the infinitesimal thermal noise variance. The threshold  $v_h$  is assumed constant during a spike, but varies from one spike to another. The distribution of  $v_h$  from spike to spike is assumed to be Gaussian or subGaussian whose parameters are estimated from experimental observations of oscillations. If the series transistor always remains in saturation and show linear voltage-current relationship, as is the case in our VO<sub>2</sub> based experiments, the discharge phase can be described by an Ornstein-Uhlenbeck (OU) process

$$dx = \frac{1}{\theta}(\mu - x)dt + \sigma dw_t \quad (4)$$

where  $\mu, \theta$  and  $\sigma$  are functions of circuit parameters of the series transistor, the IMT device and  $\sigma_t$ . The interspike interval is thus the first-passage-time (FPT) of this OU process, but with a fluctuating boundary.

Analytical expressions for the FPT of OU process (with  $\mu = 0$ ) for a constant boundary were derived using the Laplace transform method in Ref. 16. Reproducing some of its results, let the first passage time for the system (4), with  $\mu = 0$ , which starts at  $x(0) = x_0$  and hits a boundary  $S$  be denoted by the random variable  $\mathbf{t}_f(S, x_0)$ , and its  $m^{\text{th}}$  moment by  $\tau_m(S, x_0)$ . Also, let  $\tilde{\mathbf{t}}_f(S, x_0)$  be the FPT for another OU process with  $\mu = 0$ ,  $\theta = 1$  and  $\sigma = 2$ , and  $\tilde{\tau}_m(S, x_0)$  be its  $m^{\text{th}}$  moment. Then time and space scaling for the OU process imply that

$$\begin{aligned} \mathbf{t}_f(S, x_0) &\stackrel{d}{=} \theta \tilde{\mathbf{t}}_f(\alpha S, \alpha x_0) \\ \therefore \tau_m(S, x_0) &= \theta^m \tilde{\tau}_m(\alpha S, \alpha x_0) \end{aligned} \quad (5)$$

where  $\alpha = \sqrt{\frac{2}{\theta\sigma^2}}$ . The first 2 moments for the base case OU process  $\tilde{\tau}_1$  and  $\tilde{\tau}_2$  are given by

$$\begin{aligned} \tilde{\tau}_1(S, x_0) &= \phi_1(S) - \phi_1(x_0) \\ \tilde{\tau}_2(S, x_0) &= 2\phi_1(S)^2 - \phi_2(S) \\ &\quad - 2\phi_1(S)\phi_1(x_0) + \phi_2(x_0) \end{aligned} \quad (6)$$

where  $\phi_k(z)$  can be written as an infinite sum

$$\phi_k(z) = \frac{1}{2^k} \sum_{n=1}^{\infty} \frac{(\sqrt{2}z)^n \Gamma(\frac{n}{2}) \rho(n, k)}{n!} \quad (7)$$

with  $\rho(n, k)$  being a function of the digamma function [16].

We extend this framework for calculating the FPT statistics with a fluctuating boundary  $\mathbf{S}$  as follows. Let the IMT threshold be represented by the random variable  $\mathbf{v}_h$ . For the VO<sub>2</sub> based IMT neuron, the 1D subsystem in the insulating phase can be converted in the form of (4) with  $\mu = 0$  by translating the origin to the fixed point. If this transformation is  $\mathbf{T}$  then  $x = \mathbf{T}v_i$ ,  $\mathbf{S} = \mathbf{T}\mathbf{v}_h$  and  $x_0 = \mathbf{T}v_l$ . The start and end points are B' and A respectively in figure 2.  $\mathbf{v}_h$  is assumed constant during a spike, and across spikes the distribution of  $\mathbf{v}_h$  is  $\mathbf{v}_h \sim \mathcal{D}$ , where  $\mathcal{D}$  is either Gaussian, or subGaussian. For subGaussian distributions we use the Exponential Power family EP $[\kappa, \kappa$

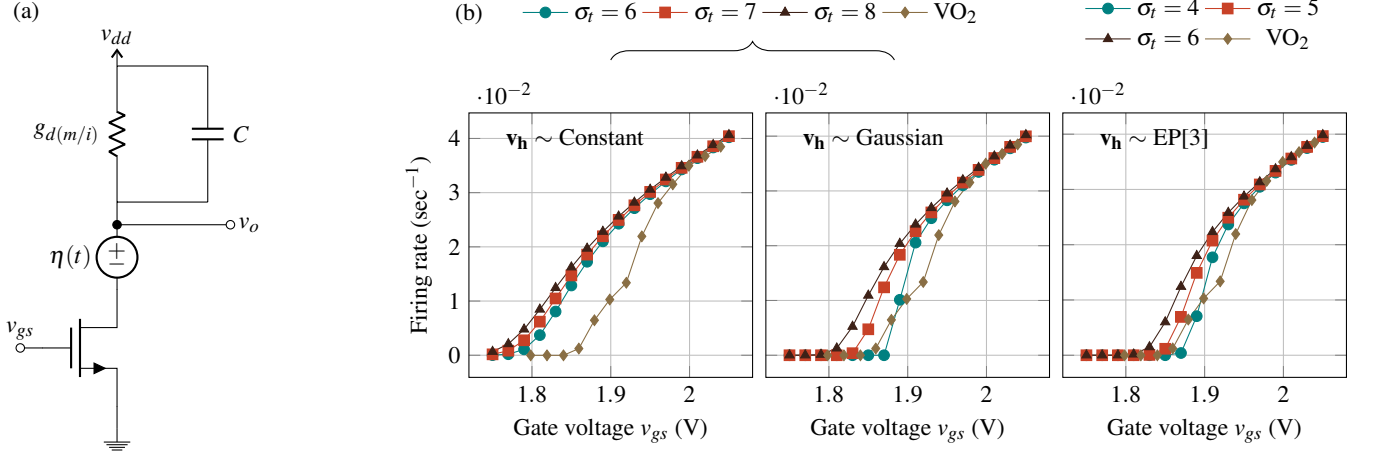


Figure 5. (a) Noise model of IMT neuron where the noise components are the thermal noise voltage source  $\eta(t)$  and the IMT threshold fluctuation. (b) Firing rate plotted against  $v_{gs}$  using the analytical model for different  $v_h$  distributions (Constant, Gaussian, and EP[3]) and comparison with experimental observations.

being the shape factor. Let the interspike interval of IMT neuron be denoted by the marginal random variable  $\mathbf{t}_{imt}(\mathcal{D}, v_l)$ . Then  $\mathbf{t}_{imt}$  is related to  $\mathbf{t}_f$  in equation (5), given common parameters  $\theta$  and  $\sigma$ , as follows:

$$\mathbf{t}_{imt}(\mathcal{D}, v_l) | (v_h = v) \stackrel{d}{=} \mathbf{t}_f(Tv, Tv_l)$$

The moments of  $\mathbf{t}_{imt}$  can be calculated as:

$$\begin{aligned} \mathbb{E}[\mathbf{t}_{imt}(\mathcal{D}, v_l)^m] &= \mathbb{E}_{v_h}[\mathbb{E}[\mathbf{t}_{imt}(\mathcal{D}, Tv_l)^m | v_h = v]] \\ &= \mathbb{E}_{v_h}[\tau_m(Tv_h, Tv_l)] \\ &= \theta^m \mathbb{E}_{v_h}[\tilde{\tau}_m(\alpha Tv_h, \alpha Tv_l)] \end{aligned} \quad (8)$$

where  $\alpha = \sqrt{\frac{2}{\theta\sigma^2}}$ . If  $\mathcal{D}$  is Gaussian or EP[ $\kappa$ ] distribution and  $\alpha T$  is an affine transformation, then  $\alpha Tv_h$  also has a Gaussian or EP[ $\kappa$ ] distribution.

First moment of  $\mathbf{t}_{imt}$  is calculated using (6) and (8) as

$$\mathbb{E}[\mathbf{t}_{imt}(\mathcal{D}, v_l)] = \theta(\mathbb{E}_{v_h}[\phi_1(\alpha Tv_h)] - \phi_1(\alpha x_0))$$

The expansion for  $\phi_k(z)$  in (7) can be used to calculate  $\mathbb{E}_{v_h}[\phi_k(\alpha Tv_h)]$  using the moments of  $\alpha Tv_h$  as follows

$$\mathbb{E}_{v_h}[\phi_k(\alpha Tv_h)] = \frac{1}{2^k} \sum_{n=1}^{\infty} \frac{(\sqrt{2})^n \mathbb{E}[(\alpha Tv_h)^n] \Gamma(\frac{n}{2}) \rho(n, k)}{n!}$$

Figure 5b shows firing rate ( $1/\mathbb{E}[\mathbf{t}_{imt}(\mathcal{D}, v_l)]$ ) as a function of  $v_{gs}$  for various  $\sigma_t$  values and for 3 distributions of threshold fluctuations. The calculations approximate the experimental observations well for all three  $v_h$  distributions, the closest being EP[3] with  $\sigma_t = 4$ .

For higher moments, higher order terms are encountered. For example, in case of the second moment, using (6) and (8), we obtain

$$\begin{aligned} \mathbb{E}_{v_h}[\tilde{\tau}_2(\alpha Tv_h, \alpha Tv_l)] &= 2\mathbb{E}_{v_h}[\phi_1(\alpha Tv_h)^2] - \mathbb{E}_{v_h}[\phi_2(\alpha Tv_h)] \\ &\quad - 2\mathbb{E}_{v_h}[\phi_1(\alpha Tv_h)]\phi_1(\alpha Tv_l) \\ &\quad + \phi_2(\alpha Tv_l) \end{aligned}$$

with a higher order term  $\phi_1(\alpha Tv_h)^2$ . In the case of the third moment we obtain  $\phi_1(\alpha Tv_h)\phi_2(\alpha Tv_h)$ . As each  $\phi_k$  term is an infinite sum, we construct a cauchy product expansion for the higher order term using the infinite sum expansions of the constituent  $\phi_k$ s and then distribute the expectation over addition. For example, if the  $\phi_k$  expansions of  $\phi_1(z)$  and  $\phi_2(z)$  are  $(\sum a_i)$  and  $(\sum b_i)$  respectively, then the cauchy product expansion of  $\phi_1(z)\phi_2(z)$  can be calculated as  $\sum c_i$ , where  $c_i$  is a function of  $a_{1\dots i}$  and  $b_{1\dots i}$ , and the expectation  $\mathbb{E}[\phi_1(z)\phi_2(z)] = \sum \mathbb{E}[c_i]$ . Since  $c_i$  is a polynomial in  $z$ ,  $\mathbb{E}[c_i]$  can be calculated using the moments of  $z$ .

If  $\mu_{imt}$  and  $\sigma_{imt}$  are the mean and standard deviation of interspike intervals  $\mathbf{t}_{imt}$ , the coefficient of variation ( $\sigma_{imt}/\mu_{imt}$ ) varies with the relative proportion of the thermal and the threshold induced noise. Figure 6 shows  $\sigma_{imt}/\mu_{imt}$  (calculated using parameters matched with our  $VO_2$  experiments) plotted against  $\sigma_t$  for various kinds of  $v_h$  distributions fitted to experimental observations.  $\sigma_{imt}/\mu_{imt}$  as observed in our  $VO_2$  experiments is about an order of magnitude more than what would be calculated with only thermal noise using such a neuron, and hence, threshold noise contributes significant stochasticity to the spiking behavior. As the IMT neuron is setup such that the stable point is close to the IMT transition point (figure 3b), low  $\sigma_t$  results in high and diverging  $\sigma_{imt}/\mu_{imt}$  for any distribution of threshold noise, and  $\sigma_{imt}/\mu_{imt}$  reduces with increasing  $\sigma_t$  for the range shown. For a Normally distributed  $v_h$  the variance diverges for  $\sigma_t \lesssim 8$ , but for Exponential Power (EP) distributions with lighter tails, the variance converges for smaller values of  $\sigma_t$ . Statistical measurements on experimental data, as indicated in figure 6, provide measures of  $\sigma_{imt}/\mu_{imt}$  (dotted line) and  $\sigma_t$  (shaded region). We note that EP distributions provide a better approximation of the stochastic nature of experimentally demonstrated  $VO_2$  neurons as the range of  $\sigma_t$  is estimated to be less than 5.

In conclusion, we demonstrate a stochastic IMT neuron which relies on threshold fluctuations and thermal noise as

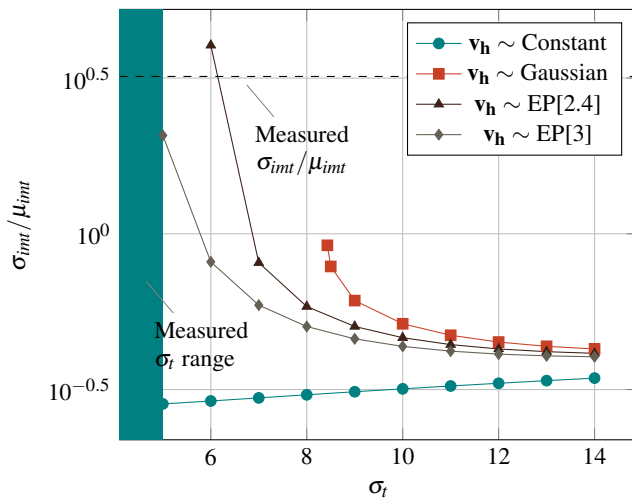


Figure 6.  $\sigma_{int}/\mu_{int}$  for the interspike interval plotted against  $\sigma_{\tau}$  for  $v_{gs} = 1.8V$  with Constant, Gaussian and Exponential Power (EP[ $\kappa$ ], where  $\kappa$  is the shape factor) distributions of the threshold noise. The experimentally observed  $\sigma_{int}/\mu_{int}$  for a VO<sub>2</sub> neuron is shown with a dotted line. The shaded region shows the experimentally estimated range of  $\sigma_{\tau}$  ( $\sigma_{\tau} < 5$ )

precursors to bifurcation. Analytical models are developed to explain the experimental observations; and we show that the neuron dynamics follow a linear “caricature” of the FitzHugh-Nagumo model with intrinsic stochasticity. With a growing consensus that stochasticity will play a key role in solving hard computing tasks, we need efficient ways for controlled amplification and conversion of physical noise into a readable and computable form. In this regard, the IMT based neuron represents a promising solution for a stochastic computational element. Such stochastic neurons have the potential to realize bio-mimetic computational kernels that can be employed to solve a large class of optimization and machine-learning problems.

**Acknowledgements:** This project was supported by the National Science Foundation under grant 1640081, and the Nanoelectronics Research Corporation (NERC), a wholly-owned subsidiary of the Semiconductor Research Corporation (SRC), through Extremely Energy Efficient Collective Electronics (EXCEL), an SRC-NRI Nanoelectronics Research Initiative under Research Task IDs 2698.001 and 2698.002.

---

[1] Simon S. Haykin. *Neural Networks and Learning Machines*. Prentice Hall, 2009.

[2] Wulfram Gerstner and Werner M. Kistler. *Spiking Neuron Models: Single Neurons, Populations, Plasticity*. Cambridge university press, 2002.

[3] Lars Buesing, Johannes Bill, Bernhard Nessler, and Wolfgang Maass. Neural Dynamics as Sampling: A Model for Stochastic Computation in Recurrent Networks of Spiking Neurons. *PLOS Comput Biol*, 7(11):e1002211, November 2011.

[4] M. Jerry, A. Parihar, B. Grisafe, A. Raychowdhury, and

S. Datta. Ultra-low power probabilistic imt neurons for stochastic sampling machines. In *Proc. Symp. VLSI Technology*, pages T186–T187, June 2017.

[5] Nikhil Shukla, Abhinav Parihar, Eugene Freeman, Hanjong Paik, Greg Stone, Vijaykrishnan Narayanan, Haidan Wen, Zhonghou Cai, Venkatraman Gopalan, Roman Engel-Herbert, Darrell G. Schlom, Arijit Raychowdhury, and Suman Datta. Synchronized charge oscillations in correlated electron systems. *Scientific Reports*, 4:4964, May 2014.

[6] N. Shukla, A. Parihar, M. Cotter, M. Barth, X. Li, N. Chandramoorthy, H. Paik, D. G. Schlom, V. Narayanan, A. Raychowdhury, and S. Datta. Pairwise coupled hybrid vanadium dioxide-MOSFET (HVFET) oscillators for non-boolean associative computing. In *2014 IEEE International Electron Devices Meeting*, pages 28.7.1–28.7.4, December 2014.

[7] Abhinav Parihar, Nikhil Shukla, Suman Datta, and Arijit Raychowdhury. Synchronization of pairwise-coupled, identical, relaxation oscillators based on metal-insulator phase transition devices: A model study. *Journal of Applied Physics*, 117(5):054902, February 2015.

[8] Ayan Kar, Nikhil Shukla, Eugene Freeman, Hanjong Paik, Huichu Liu, Roman Engel-Herbert, S. S. N. Bharadwaja, Darrell G. Schlom, and Suman Datta. Intrinsic electronic switching time in ultrathin epitaxial vanadium dioxide thin film. *Applied Physics Letters*, 102(7):072106, 2013.

[9] Matthew Jerry, Nikhil Shukla, Hanjong Paik, Darrell G Schlom, and Suman Datta. Dynamics of electrically driven subnanosecond switching in vanadium dioxide. In *Silicon Nanoelectronics Workshop (SNW), 2016 IEEE*, pages 26–27. IEEE, 2016.

[10] TL Cocker, LV Titova, S Fourmaux, G Holloway, H-C Bandulet, D Brassard, J-C Kieffer, MA El Khakani, and FA Hegmann. Phase diagram of the ultrafast photoinduced insulator-metal transition in vanadium dioxide. *Physical Review B*, 85(15):155120, 2012.

[11] A. Tonnelier. The McKean’s Caricature of the Fitzhugh–Nagumo Model I. The Space-Clamped System. *SIAM Journal on Applied Mathematics*, 63(2):459–484, January 2003.

[12] H. P McKean. Nagumo’s equation. *Advances in Mathematics*, 4(3):209–223, June 1970.

[13] M. di Bernardo, A. Nordmark, and G. Olivar. Discontinuity-induced bifurcations of equilibria in piecewise-smooth and impacting dynamical systems. *Physica D: Nonlinear Phenomena*, 237(1):119–136, January 2008.

[14] Matthew Jerry, Abhinav Parihar, Arijit Raychowdhury, and Suman Datta. A random number generator based on insulator-to-metal electronic phase transitions. In *Device Research Conference (DRC), 2017 75th Annual*, pages 1–2. IEEE, 2017.

[15] Kailiang Zhang, Baolin Wang, Fang Wang, Yemei Han, Xiaochuan Jian, Hongzhi Zhang, and HS Philip Wong. Vo 2-based selection device for passive resistive random access memory application. *IEEE Electron Device Letters*, 37(8):978–981, 2016.

[16] Luigi M. Ricciardi and Shunsuke Sato. First-Passage-Time Density and Moments of the Ornstein-Uhlenbeck Process. *Journal of Applied Probability*, 25(1):43–57, 1988.